Journal of Organometallic Chemistry 696 (2011) 1887–1894

Contents lists available at ScienceDirect

Journal of Organometallic Chemistry

journal homepage: www.elsevier.com/locate/jorganchem

Synthesis of and ethylene oligomerization with binuclear palladium catalysts having sterically modulated bis-imine ligands with methylene spacer

Srinivasa Budagumpi [a], Yinshan Liu [a], Hongsuk Suh [b], Il Kim [a,*]

[a] The WCU Center for Synthetic Polymer Bioconjugate Hybrid Materials, Division of Chemical Engineering, Pusan National University, Pusan 609-735, Republic of Korea
[b] Department of Chemistry and Chemistry Institute for Functional Materials, Pusan National University, Pusan 609-735, Republic of Korea

ARTICLE INFO

Article history:
Received 12 January 2011
Received in revised form
23 February 2011
Accepted 1 March 2011

Keywords:
Binuclear
Bis-imine ligand
Catalysis
Ethylene oligomerization
Palladium
Transition metal chemistry

ABSTRACT

Sterically modulated bis-imine ligands (L^1–L^3) were prepared by reacting 4,4′-methylene bis-(2,6-dialkyl aniline) and antipyrine-4-carboxaldehyde in a 1:2 stoichiometric ratio. The reactions of L^1–L^3 with dichloro(cycloocta-1.5-diene)palladium(II) [$PdCl_2$(cod)] yield the corresponding binuclear palladium complexes with the general formula Pd_2Cl_4L (L = L^1, L^2, and L^3). The binucleating ligands bind to the palladium ion via the lone pair on the imine nitrogen and amide oxygen atoms, resulting in a square-planar geometry around the metal center. All the palladium catalysts efficiently oligomerize ethylene to produce C_4–C_{20} fractions at activities of up to 1308 kg-oligomer mol-Pd^{-1} bar^{-1} h^{-1} at 30 °C in combination with ethylaluminum sesquichloride. The formation of active sites by the change in geometry of the metal complexes could be traced using spectroscopic and electrochemical techniques.

1. Introduction

In the past decade, a new generation of oligomerization catalyst precursors has emerged with excellent activity, selectivity, living behavior, and stability [1–3]. In particular, ethylene oligomerization systems have been reported for nickel, iron, and chromium, but palladium-based catalysts constitute the most numerous, active, and selective group. Essentially, non-metallocene bis-imine based catalysts comprising of a bimetallic core separated by aliphatic or aromatic spacers were employed to achieve synergistic effects found in metallocene catalysts [4,5]. The ligand design of such systems is of fundamental importance, because the ligand structure defines the environment around the metal centers. Broadly speaking, there are two different types of bimetallic cores: a remote donor bimetallic core with aliphatic or aromatic spacers and an atom- or bond-bridged core. The former is of greater interest because the distance between the metals can be tuned using extended pi-bond conjugations through the spacers. Bimetallic palladium catalysts offer diverse and difficult challenges with regards to the design of new efficient catalyst systems for ethylene oligomerization. Linear α-olefins have a wide range of applications [6]. The lower carbon numbers are overwhelmingly used as comonomers in the production of polyethylene. C_4–C_8 linear α-olefins are used in the synthesis of linear aldehydes via hydroformylation reactions. They have also been employed in the production of poly-α-olefin synthetic lubricant base stock and surfactants. Higher linear α-olefins are used in making surfactants for aqueous detergent formulations and hydrophobes in oil-soluble surfactants. At present, even-carbon-numbered α-olefins are produced industrially, but mostly via non-selective oligomerization of ethylene [6].

The rapid expansion of this area, stimulated by the promising catalytic activity of palladium complexes, resulted in considerable contributions to polyethylene production. Antipyrene-4-carboxaldehyde is of particular interest due to the feasibility and flexibility of ligand design, which allows the introduction of sterically and electronically demanding features [7,8]. Phenyl and alkyl groups attached adjacent to functional chromophores such as amide carbonyls and aldehyde groups in the antipyrine ring make the derived ligand systems active for ethylene oligomerization. The required degree of hindrance can be obtained using the alkyl and phenyl groups, allowing chain termination after the formation of the desired oligomers. In order to achieve variable steric hindrance in the ligand systems, a series of bis-amines with different aliphatic groups can be used [9]. The most notable feature of the catalysts formed by these combinations is the presence of fixed methyl and phenyl substituents on one side of the metal and variable aliphatic substitutions on the other side, which makes these ligands very

* Corresponding author. Tel.: +82 51 5102466; fax: +82 51 5137720.
E-mail address: ilkim@pusan.ac.kr (I. Kim).

0022-328X/$ – see front matter © 2011 Elsevier B.V. All rights reserved.
doi:10.1016/j.jorganchem.2011.03.003

suitable for ethylene oligomerization [4,10]. In this regard, a series of simple bis-imine ligands derived from 4,4′-methylene bis-(2,6-dialkyl aniline) and antipyrine-4-carboxaldehyde were studied for the preparation of palladium catalysts, resulting in bidentate ligation and a square-planar Pd coordination. As a continuation of our research into these catalysis, we herein report interesting results regarding ethylene oligomerization with a series of sterically modulated palladium catalysts.

2. Experimental

2.1. Materials for the preparation of catalysts

All reactions were performed under a purified nitrogen atmosphere using the standard Schlenk technique. Polymerization-grade ethylene (SK Co., Korea) was purified by passing through columns of Fisher RIDOX™ catalyst and molecular sieves 5A/13X Organic solvents, namely, ethanol, methanol, and diethyl ether, were distilled over CaH_2 and stored over molecular sieves. Toluene was distilled over Na/benzophenone under nitrogen and stored over molecular sieves. The reagents antipyrine-4-carboxaldehyde, dichloro(cycloocta-1.5-diene)palladium(II) [$PdCl_2$(cod)], 4,4′-methylene bis-(2,6-dimethyl aniline), 4,4′-methylene bis-(2,6-diethyl aniline), 4,4′-methylene bis-(2,6-diisopropyl aniline), and glacial acetic acid were purchased from Aldrich Chem. Co. and used without further purification. Unless noted otherwise, all reagents were purchased from commercial sources and used as received.

2.2. Physical methods

^{1}H and ^{13}C NMR spectra were recorded in $CDCl_3$ solvent on a Varian Gemimi-2000 300 MHz spectrometer at room temperature using TMS as an internal reference. Analytical thin layer chromatography (TLC) was carried out using Merck 0.25 mm silica gel 60F pre-coated aluminum plates with fluorescent indicator UV254. All ligands were purified using a Combi-Flash (Companion) auto-column machine. Elemental analysis was carried out using a Vario EL analyzer. Infrared (IR) spectra were recorded as KBr discs (ligands) or CsI (catalysts) disc matrix using a Shimadzu IRPrestige-21 over a 4000–200 cm^{-1} range. The electronic spectra of the complexes were recorded on a Shimadzu UV-1650PC spectrophotometer in the range of 1000–200 nm. Cyclic voltammetry (CV) studies were performed at room temperature in chloroform under O_2 free conditions using Kosentech Model CV-104. Mass spectra of catalysts were recorded using positive fast atom bombardment (FAB) methods on a JEOL JMS-700, HP 5890 Series II spectrometer. Thermogravimetric (TG) and differential thermal analysis (DTA) of the catalysts were performed under a nitrogen atmosphere on a DuPont 951 maintaining the final temperature at 800 °C and a heating rate of 10 °C/min under a nitrogen atmosphere. The oligomers were analyzed by gas chromatography (HP–6890) using a J&W Scientific DB608 column (30 mm 90.53 mm) equipped with a FID detector. The injector and detector temperature was kept constant at 250 °C. The initial temperature was set at 30 °C (hold 2 min) and finishing temperature at 250 °C (hold 10 min) with a heating rate of 10 °C/min.

2.3. Ethylene oligomerization

Ethylene oligomerization was performed in a 250 mL round-bottom flask equipped with a magnetic stirrer and a thermometer. High-dilution techniques were adopted to reduce the monomer mass transport effect. After addition of the catalyst, the reactor was charged with toluene (80 mL) via a syringe and immersed in a constant temperature bath previously set to a desired temperature. When the reactor was equilibrated to the bath temperature, ethylene was pressurized into the reactor (1.3 bar) after removing the nitrogen gas under vacuum. When no more absorption of ethylene into toluene was observed, a prescribed amount of co-catalyst was injected into the reactor and oligomerization commenced. The oligomerization rate was determined every 0.01 s from the rate of consumption, measured by a hotwire flow meter (model 5850 D from Brooks Instrument Div.) connected to a PC through an A/D converter. Oligomerization was quenched by the addition of methanol containing HCl (5 v/v%) after cooling. The resulting mixture was passed through an alumina column to remove all aluminum containing species and the obtained oligomers were analyzed by gas chromatography. The rate of ethylene consumption was directly obtained from the computerized experimental apparatus and is expressed as in terms of g-product mol-Pd^{-1} h^{-1} bar^{-1}. In order to make a convincing assessment of the effects of catalyst structure on catalytic activity and oligomer distribution, all data were collected under similar conditions.

2.4. Detection of the active species

2.4.1. ^{1}H NMR spectral technique

Alkyl-palladium active species were detected by *in-situ* ^{1}H NMR spectral technique under ethylene oligomerization conditions. Palladium catalyst (2.5 μmol) was introduced into an NMR tube under a nitrogen atmosphere and deuterated chloroform (0.7 mL) was added. The tube was saturated with ethylene gas, followed by the addition of ethylaluminum sesquichloride (EASC) (Al/Pd = 300). The ^{1}H NMR spectra of the reaction mixture was recorded as a function of time. The changes observed were correlated with a blank EASC spectrum as a control under similar conditions.

2.4.2. Electronic spectral technique

For the detection of alkyl-palladium active species formed during oligomerization, UV–visible spectra of the catalysts were recorded under oligomerization conditions. Palladium catalyst (2.5 μmol) was added to a cuvette containing 1 mL of toluene in an inert atmosphere, and then saturated with ethylene gas (1.3 bar). EASC (Al/Pd = 300) was injected into the system to initiate oligomerization and the UV–visible spectra of the reaction mixture were recorded over time.

2.5. Syntheses

2.5.1. Preparation of the ligands (L^1–L^3)

A methanolic solution of antipyrine-4-carboxaldehyde (0.432 g, 2 mmol) was added to a methanolic solution of 4,4′-methylene bis-(2,6-dimethyl aniline) (0.254 g, 1 mmol) in a 50 mL Schlenk flask under a nitrogen atmosphere. A catalytic amount of formic acid was added and the reaction mixture was kept at refluxing temperature for 4 h, and then cooled to room temperature. A pale yellow solid was separated by filtration and purified by column chromatography using hexane/ethyl acetate as eluant (8:2 v/v). The product (L^1) was dried under vacuum at room temperature and stored in a vacuum desiccator. The reactions involved in the preparation of the ligands are outlined in Fig. 1. Yield: 46.3%. m.p.: 109–111 °C. Elemental analysis: Found (calculated) for $C_{41}H_{42}N_6O_2$: C 75.4 (75.7), H 6.9 (6.5), N 12.1 (12.9). FTIR (KBr disc) cm^{-1}: 3384 ν (N–C, antipyrine ring), 2922 ν (C–H, alkyl), 1676 ν (>C=O, amide), 1599 ν (>C=N, imine), and 1076 ν (N–N, antipyrine ring). ^{1}H NMR ($CDCl_3$) ppm: 8.4 (s, 2H, azomethine protons), 7.8–7.4 (m, 10H, aromatic protons), 6.9 (s, 4H, aromatic protons), 3.6 (s, 2H, methylene spacer protons), 3.1 (s, 6H, antipyrine N–Me protons), 2.4 (s, 6H, antipyrine C–Me protons), and 1.0 (s, 12H, methyl protons). ^{13}C NMR ($CDCl_3$) ppm:

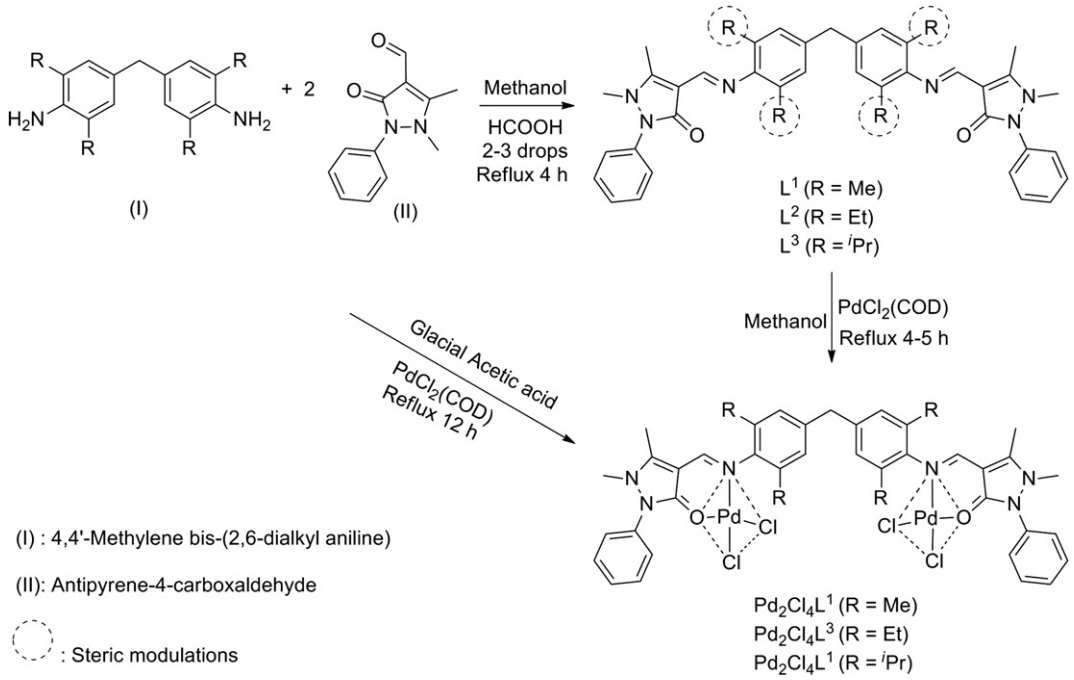

Fig. 1. Preparation of sterically modulated ligands and Pd catalysts.

168 (>C═O amide), 149 (>C═N imine), 121, 119, 116, 109 (aromatic region), 77 (antipyrine N–Me methyl), 53 (antipyrine C–Me methyl), and 24 (methyl). UV–vis (MeOH) nm: 278 ($\pi-\pi^*$ of C═N) and 303 ($n-\pi^*$ of N and O).

L^2 was similarly prepared using 4,4′-methylene bis-(2,6-diethyl aniline) (0.31 g, 1 mmol). Yield: 41.4%. m.p.: 172–174 °C. Elemental analysis: Found (calculated) for $C_{45}H_{50}N_6O_2$: C 75.9 (76.5), H 7.4 (7.1), N 12.2 (11.9). FTIR (KBr disc) cm^{-1}: 3397 ν (N–C, antipyrine ring), 2916 ν (C–H, alkyl), 1681 ν (>C═O, amide), 1601 ν (>C═N, imine), and 1092 ν (N–N, antipyrine ring). ^1H NMR ($CDCl_3$) ppm: 8.1 (s, 2H, azomethine protons), 7.6–7.0 (m, 10H, aromatic protons), 6.6 (s, 4H, aromatic protons), 3.9 (s, 2H, methylene spacer protons), 3.2 (s, 6H, antipyrine N–Me protons), 1.9 (s, 6H, antipyrine C–Me protons), 1.4 (q, 8H, methylene protons), and 0.7 (t, 12H, methyl protons). ^{13}C NMR ($CDCl_3$) ppm: 171 (>C═O amide), 148 (>C═N imine), 124, 122, 116, 112 (aromatic region), 79 (antipyrine N–Me methyl), 43 (antipyrine C–Me methyl), 40 (methylene), and 21 (methyl). UV–vis (MeOH) nm: ~270 ($\pi-\pi^*$ of C═N) and ~300 ($n-\pi^*$ of N and O).

L^3 was similarly prepared using 4,4′-methylene bis-(2,6-diisopropyl aniline) (0.366 g, 1 mmol). Yield: 38.1%. m.p.: 198 °C. Elemental analysis: Found (calculated) for $C_{49}H_{58}N_6O_2$: C 77.6 (77.2), H 7.4 (7.7), N 11.6 (11.0). FTIR (KBr disc) cm^{-1}: 3371 ν (N–C, antipyrine ring), 2920 ν (C–H, alkyl), 1680 ν (>C═O, amide), 1604 ν (>C═N, imine), and 1047 ν (N–N, antipyrine ring). ^1H NMR ($CDCl_3$) ppm: 8.3 (s, 2H, azomethine protons), 7.8–7.1 (m, 10H, aromatic protons), 6.8 (s, 4H, aromatic protons), 4.1 (s, 2H, methylene spacer protons), 3.5 (s, 6H, antipyrine N–Me protons), 2.0 (s, 6H, antipyrine C-Me protons), 2.4 (sept, 4H, isopropyl protons) and, 0.8 (d, 24H, methyl protons). ^{13}C NMR ($CDCl_3$) ppm: 176 (>C═O amide), 152 (>C═N imine), 125, 121, 118, 110 (aromatic region), 79 (antipyrine N–Me methyl), 48 (antipyrine C–Me methyl), 44 (isopropyl), 40 (methylene), and 31 (methyl). UV–vis (MeOH) nm: ~275 ($\pi-\pi^*$ of C═N) and ~300 ($n-\pi^*$ of N and O).

2.5.2. Preparation of binuclear palladium complexes

For the preparation of $Pd_2Cl_4L^1$, a methanolic solution of $PdCl_2$ (cod) (4 mmol) was added drop wise to a solution of L^1 ligand (2 mmol) in methanol (15 mL) over a period of 30 min. The reaction mixture was refluxed for 4–5 h, cooled to room temperature, and then the resultant mixture was precipitated in diethyl ether. The filtered solids were washed with methanol and ether to remove traces of metal salt and finally dried and stored under vacuum. Yield: 79.7%. m.p.: >300 °C. Elemental analysis: Found (calculated) for $C_{41}H_{42}N_6O_2Pd_2Cl_4$: C 49.4 (49.0), H 4.7 (4.2), N 8.1 (8.4). FTIR (KBr disc) cm^{-1}: ~3380 ν (N–C, antipyrine ring), 2920 ν (C–H, alkyl), 1653 ν (>C═O, amide), 1610 ν (>C═N, imine), 1070 ν (N–N, antipyrine ring), and 422 ν (Pd–N). ^1H NMR ($CDCl_3$) ppm: 8.5 (s, 2H, azomethine protons), 7.7–7.0 (m, 10H, aromatic protons), 6.9 (s, 4H, aromatic protons), 4.1 (s, 2H, methylene spacer protons), 3.0 (s, 6H, antipyrine N–Me protons), 2.4 (s, 6H, antipyrine C–Me protons), and 0.9 (s, 12H, methyl protons). ^{13}C NMR ($CDCl_3$) ppm: 184 (>C═O amide), 153 (>C═N imine), 120, 116, 111, 109 (aromatic region), 75 (antipyrine N–Me methyl), 50 (antipyrine C–Me methyl), and 24 (methyl). UV–vis (MeOH) nm: 290 ($\pi-\pi^*$ of C═N) and 310 ($n-\pi^*$ of N and O). FAB mass (m/z): 935 ($M^+ - Cl$).

$Pd_2Cl_4L^2$: Yield: 79.7%. m.p.: >300 °C. Elemental analysis: Found (calculated) for $C_{45}H_{50}N_6O_2Pd_2Cl_4$: C 50.4 (50.9), H 4.9 (4.8), N 8.2 (7.9). FTIR (KBr disc) cm^{-1}: ~3390 ν (N–C, antipyrine ring), 2920 ν (C–H, alkyl), 1658 ν (>C═O, amide), 1610 ν (>C═N, imine), ~1090 ν (N–N, antipyrine ring), and 434 ν (Pd–N). ^1H NMR ($CDCl_3$) ppm: 8.0 (s, 2H, azomethine protons), 7.6–7.1 (m, 10H, aromatic protons), 6.8 (s, 4H, aromatic protons), 4.2 (s, 2H, methylene spacer protons), 3.1 (s, 6H, antipyrine N–Me protons), 1.9 (s, 6H, antipyrine C–Me protons), 1.8 (q, 8H, methylene protons), and 0.9 (t, 12H, methyl protons). ^{13}C NMR ($CDCl_3$) ppm: 180 (>C═O amide), 151 (>C═N imine), 126, 122, 119, 111 (aromatic region), 82 (antipyrine N–Me methyl), 42 (antipyrine C–Me methyl), 40 (methylene), and 27 (methyl). UV–vis (MeOH) nm: ~290 ($\pi-\pi^*$ of C═N) and 305 ($n-\pi^*$ of N and O). FAB mass (m/z): 991 ($M^+ - Cl$).

$Pd_2Cl_4L^3$: Yield: 79.7%. m.p.: >300 °C. Elemental analysis: Found (calculated) for $C_{49}H_{58}N_6O_2Pd_2Cl_4$: C 52.8 (52.3), H 5.4 (5.0), N 7.2 (7.6). FTIR (KBr disc) cm^{-1}: ~3370 ν (N–C, antipyrine ring), 2922 ν (C–H, alkyl), 1648 ν (>C═O, amide), 1611 ν (>C═N, imine), ~1040 ν (N–N, antipyrine ring), and 436 ν (Pd–N). ^1H NMR ($CDCl_3$) ppm: 8.3 (s, 2H, azomethine protons), 7.7–7.2 (m, 10H, aromatic protons), 6.9

(s, 4H, aromatic protons), 4.2 (s, 2H, methylene spacer protons), 3.3 (s, 6H, antipyrine N–Me protons), 2.0 (s, 6H, antipyrine C–Me protons), 2.4 (sept, 4H, isopropyl protons), and 0.9 (d, 24H, methyl protons). ^{13}C NMR ($CDCl_3$) ppm: 183 (>C=O amide), 156 (>C=N imine), 129, 120, 118, 103 (aromatic region), 72 (antipyrine N–Me methyl), 43 (antipyrine C–Me methyl), 38 (isopropyl), 31 (methylene), and 24 (methyl). UV–vis (MeOH) nm: ~280 (π–π^* of C=N) and ~295 (n–π^* of N and O). FAB mass (m/z): 1047 ($M^+ - Cl$).

2.5.3. Preparation of palladium complexes by in-situ method

The disconcertingly low yields of the ligands prompted us to attempt to prepare the catalysts by an *in-situ* method. For example, 4,4′-methylene bis-(2,6-dialkyl aniline) (1 mmol), antipyrine-4-carboxaldehyde (2 mmol) and $PdCl_2$ (cod) were added to 25 mL glacial acetic acid in a 50 mL Schlenk flask under a nitrogen atmosphere. The reaction mixture was refluxed over a period of 12 h and cooled to room temperature. The resultant mixture was precipitated in diethyl ether. The filtered solids were washed with methanol and ether to remove traces of metal salt and finally dried and stored under vacuum. These catalysts were independently characterized as previously described; the data obtained were consistent with the structure of the catalysts prepared by the conventional method. However, the yield of the catalysts was considerably improved 30–40%.

3. Results and discussion

3.1. General characterizations and electrochemistry of the synthesized compounds

All the synthesized compounds have been thoroughly characterized by a wide range of spectro-analytical techniques to support the proposed structures. Our failure to obtain single crystals of the complexes (using different methods/solvents) may be attributed to the high amorphous nature of the complexes. The ligands prepared and their respective palladium complexes are NMR active, which allows for accurate structural characterization despite the lack of single-crystal data.

The ease in which the steric and electronic properties of the complexes are adjusted is an important feature of the group-X metal complexes when used as olefin polymerization catalysts [11–13]. In the conventional synthesis of ligands, catalytic amounts of formic acid are used to achieve an acidic pH in the reaction mixture, which facilitates the reaction of the aldehyde. A series of bis-anilines were used in order to tune the steric properties of the ligands while maintaining the antipyrine core. The ligands have been show to ligate through the imine (azomethine) nitrogen and the amide carbonyl oxygen atoms to form stable six-membered chelated rings. The ligand systems are designed in such a way that, after coordination to Pd centers, loss of labile chlorides is prevented. The aforementioned chloride elimination plays a significant role in ethylene oligo/polymerizations due to replacement of said anions with alkyl groups of aluminum co-catalysts. Dichloro Pd centers were chosen in the present work, as these derivatives possess dsp^2 hybridization and are NMR active, allowing a deeper insight into their structures.

All synthesized compounds were characterized by IR spectroscopy. Selected IR absorption bands and their corresponding assignments are given in the experimental section. Ligands L^1–L^3show two distinct bands around 1680 and 1600 cm^{-1}, attributed to amide carbonyl and imine stretching frequencies, respectively [14]. The spectra of the complexes, the amide and imine bands underwent negative and positive shifts respectively, indicating involvement in the coordination with Pd center. A few other important bands at around 3380, 2920, 1080, and 430 cm^{-1} can be ascribed to the tertiary nitrogen, alkyl C–H, diazine N–N, and Pd–N stretching frequencies, respectively.

Ligands and their Pd complexes have been characterized with the aid of ^{1}H NMR over a range of 0–14 ppm. An aldehydic proton of antipyrine-4-carboxaldehyde can be observed as a singlet at 9.8 ppm. The peak is shifted up-field to around 8.2 ppm in ligands, indicating the formation of azomethine linkage between the anilines and antipyrine-4-carboxaldehyde. However, in the Pd complex, the peak shifts down-field by 0.2–0.4 ppm, demonstrating the involvement of azomethine nitrogen in the Pd coordination. The decrease in electron density surrounding the azomethine proton after lone-pair donation from nitrogen atom transfers electron density to electropositive Pd center. This observation is also supported by ^{13}C NMR spectra of the compounds, in which azomethine carbon resonance shifts down-field in the complexes. The involvement of the amide carbonyl in the coordination is again confirmed by ^{13}C NMR spectra of the complexes, where amide carbonyl carbon resonance shifts to a down-field region. In addition, ^{1}H and ^{13}C NMR spectra of the compounds show a set of peaks in the region 7–8, 0.7–4.2 and 104–145, 21–75 ppm ascribed to the aromatic and aliphatic resonances, respectively. The NMR studies allow us to propose a structure for the complexes prepared. Pd complexes are NMR active only if they possess a square-planar geometry, hence it is assumed that, the Pd complexes synthesized possess such geometry with dsp^2 hybridization. The four corners of the plane are covered by imine nitrogen, amide oxygen and two labile chlorides in *cis*-fashion on either side of the methylene spacer.

NMR active Pd complexes with square-planar geometry, are diamagnetic in nature [15–18], thus magnetic exchange interactions through methylene spacer can be ruled-out. However, electronic interactions between both the Pd centers are possible as an extended pi-electron conjugation can be found through the spacer. These complexes may act as efficient ethylene oligomerization catalysts due to these electronic interactions found in the form of cooperative effects between Pd centers. The same effect cannot be expected in their mononuclear counterparts.

The UV–visible spectra of the compounds were recorded at room temperature in methanol solution at 10^{-3} M concentration. The electronic spectra of the ligands show two distinct bands at 275 and 305 nm. These can be assigned to the intra ligand n–π^* and n–π^* transitions of the amide carbonyl and azomethine functionalities. These bands suffered red shifts of 10–15 nm in the corresponding Pd complexes, indicating coordination of the azomethine nitrogen and amide carbonyl. UV–visible spectra of the Pd complexes are characterized by intense bands around 450 nm (ε-170 l cm^{-1} mol^{-1}), assigned to the d–d transitions of the Pd^{II} ion. This observation is consistent with values for Pd complexes reported in literature [15–18]. In case of $Pd_2Cl_4L^3$, a weak band is observed around 415 (ε-140 l cm^{-1} mol^{-1}) nm corresponding to the d–d transition of the metal ion. The electronic and diamagnetic properties collectively indicate a square-planar geometry around the Pd centers.

The FAB mass spectra of $Pd_2Cl_4L^1$, $Pd_2Cl_4L^2$, and $Pd_2Cl_4L^3$ show intense peaks for $M^+ - Cl$ at m/z 935, 991, and 1047, respectively. Apart from this, the spectra show other peaks at regular intervals after the elimination of one and two chlorides at 36 and 72 molecular weight losses with exact isotopic patterns. Further molecular fragmentation is consistent with various fragments of the complexes, with the appropriate isotopes of both Pd and Cl. The spectra indicate that all the Pd complexes are binuclear and monomeric in nature.

The thermal degradation of the Pd complexes was studied in the temperature range of 30–800 °C under a nitrogen atmosphere. As expected, there is no weight loss below 100 °C, indicating the absence of coordinated or lattice celled solvent molecules. Weight

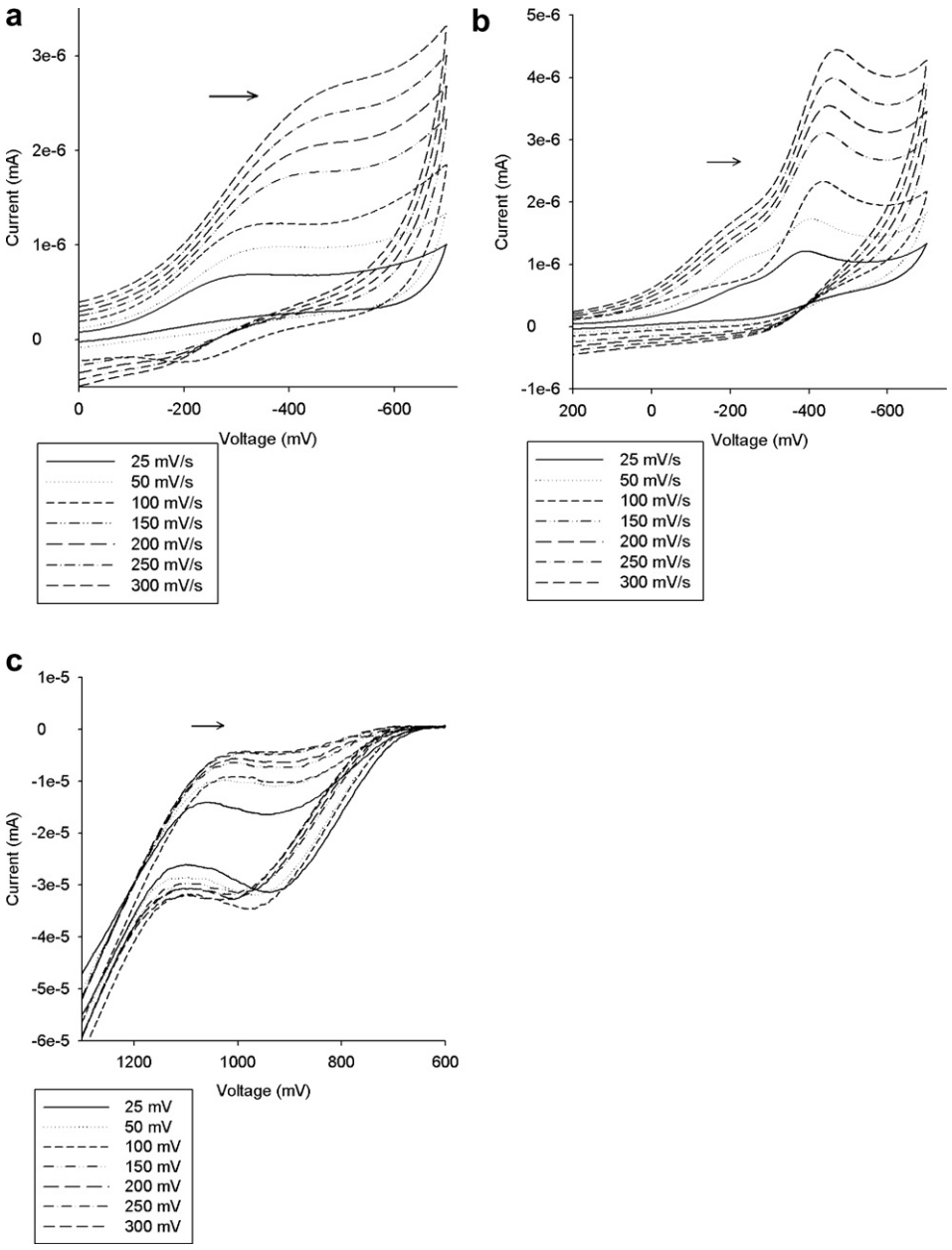

Fig. 2. Cyclic voltammograms of $Pd_2Cl_4L^1$ (a), $Pd_2Cl_4L^2$ (b), and $Pd_2Cl_4L^3$ (c) at different scan rates.

loss is observed in two significant steps for all the Pd complexes. Weight losses of 14.1%, 13.6%, and 12.9% were observed for $Pd_2Cl_4L^1$, $Pd_2Cl_4L^2$, and $Pd_2Cl_4L^3$, respectively, at 230–265 °C due to the elimination of chlorine atoms. This was further supported by the appearance of an exothermic peak at around 245 °C in the DTA signal. In the second step, 60.1%, 62.1%, and 62.9% weight loss was observed for the said series of Pd catalysts, respectively, at 410–460 °C, indicating the degradation of the ligand moiety. Finally, the graph leveled off due to the formation of the stable Pd oxide. The data obtained from thermal analysis can be correlated to the proposed structures of the Pd complexes.

The electrochemical behavior of metal complexes containing two or more chemically equivalent electro-active sites has been the subject of a number of studies in olefin oligo/polymerizations [19]. Steric modulation around the Pd centers may change the orientation of the catalyst structure and hence the potential at the metal center, which could severely impact oligomerization activity. CV measurements allow us to monitor this effect. The electrochemical characterization of Pd complexes having different substituent groups was carried out in dimethylformamide (DMF) solution at a concentration of 10^{-3} M. Tetrabutylammonium perchlorate (0.1 M) was used as supporting electrolyte and the scans were recorded under a nitrogen atmosphere, which was created by purging pure nitrogen gas through DMF solution. In the presence of aluminum co-catalysts, immediate precipitation and high adsorption at the electrode surface occurred on applying the potential. Thus, interpretation was difficult for the cyclic voltammograms obtained under conditions similar to those during ethylene oligomerization. It is reported in the literature [20] that, for the reversible sequential transfer of two electrons, the ΔEp in the cyclic voltammograms would be 42 mV. In contrast, cyclic voltammograms for molecules with multiple, non-interacting redox centers will be similar to those of the corresponding species with a single centre and ΔEp should be 58 mV [21]. However, the cyclic voltammograms of the present Pd complexes show no indication of mixed valence Pd ions.

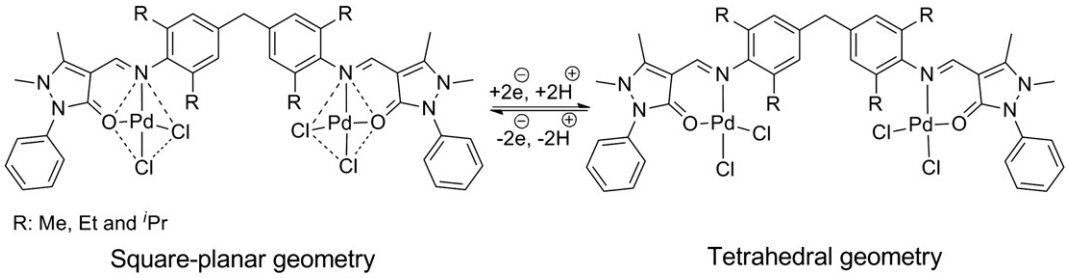

Fig. 3. Proposed one electron transfer redox behavior of the Pd complexes.

The cyclic voltammograms of the free ligands and their Pd complexes were scanned in the potential range of +2000 to −2000 mV at different scan rates viz., 25, 50, 100, 150, 200, 250, and 300 mV/s. Cyclic voltammograms of $Pd_2Cl_4L^1$, $Pd_2Cl_4L^2$, and $Pd_2Cl_4L^3$ are shown in Fig. 2a–c. In order to clarify the uncertainty regarding Pd versus ligand reduction, we examined the potentially innocent ligands L^1–L^3 in the same potential range with same scan rates, displaying no significant redox waves. This leads us to conclude that in all cases the redox processes are Pd based.

$Pd_2Cl_4L^1$ shows one electron transfer quasi-reversible redox behavior at the reported ligand field of L^1. The reduction potential of $Pd_2Cl_4L^1$ is in the range −296 to −405 mV and the corresponding oxidation potential is in the range −498 to −198 mV over the corresponding scan rates. The difference between cathodic and anodic peak potentials ΔEp is found ~95 mV for all scan rates. Similarly, the ratio of cathodic to anodic peak current (Ipa/Ipc) is found to be less than one at all scan rates, hence the system is ascribed to one electron transfer quasi-reversible process. $Pd_2Cl_4L^2$ shows a reduction peak in the range −392 to −441 mV and the corresponding oxidation potential in the range −355 to −309 mV at different scan rates. Peak-to-peak potential difference ΔEp is found at around 85 mV for all scan rates, however, the ratio of cathodic to anodic peak current (Ipa/Ipc) is less than one, indicating one electron transfer quasi-reversible redox process for the system. Peak potential difference is found to be less than the $Pd_2Cl_4L^1$ system, perhaps due to the presence of the more sterically hindered bulky ethyl group.

Interestingly, $Pd_2Cl_4L^3$ system shows one electron transfer reversible redox behavior in the working potential range and noticeably the redox peaks shifted to positive voltages in this particular case. The reduction potential for this electro-active system is shown in the range 1021–1037 mV and the corresponding oxidation potential found in the range 961–982 mV. The difference between cathodic and anodic peak potentials ΔEp is found at around 58 mV for all scan rates. Eventually, the ratio of cathodic to anodic peak current (Ipa/Ipc) is almost one, indicating one electron transfer reversible redox process for the system. The reported Pd complexes bearing different alkyl groups on either side of the anilines show different electrochemical behaviors, as a consequence of increased steric hindrance as the size of the substituent increases. The Pd complex with a methyl substitution shows more peak-to-peak difference in potential whereas the ethyl substituted complex shows less peak-to-peak difference. The isopropyl derivative lies almost in the range of a reversible process. This change in the potential of the Pd centers disturbs the geometry around the metal center (as shown in Fig. 3). The reduced Pd center assumes a tetrahedral geometry and in the reverse scan, the oxidized centers revert to the original square-planar geometry. As a result of this change in geometry and oxidation sate of the Pd centers, significant variations are expected in their ethylene oligomerization activity and in the resulting oligomer distributions (*vide infra*). It is also expected from the CV studies that the catalytic activity of the isopropyl derivatized catalyst is higher than those of the other two catalysts, since the reduced tetrahedral Pd centers may be the active species for the conversion of ethylene into its oligomers [22].

3.2. Ethylene oligomerization

The Pd complexes prepared act as efficient ethylene oligomerization catalysts as illustrated by the oligomerization rate curves (Fig. 4). The activity shown by Pd catalysts is explained in two different aspects.

The use of multi-nucleating ligands as a means of imposing close spatial confinement on multi-metal centers has been widely documented for a variety of catalysts over a range of metal-mediated processes [23–25]. For oligo/polymerization applications, good catalytic performances have been observed and cooperative effects by the neighboring active metal centers have also been suggested [26]. Brookhart and coworkers reported that the catalysts with only one substituent on the N-aryl rings for α-diimine ligands produce only oligomers [27]. Steric modulations in the methylene spacer bridged ligands affects ethylene oligomerization not only from the viewpoint of yield but also product distribution. In case of the Brookhart catalyst, the group X metal is sufficiently hindered by four isopropyl groups present at the 2,6-positions of the anilines attached to a central acenapthaquinone core. This

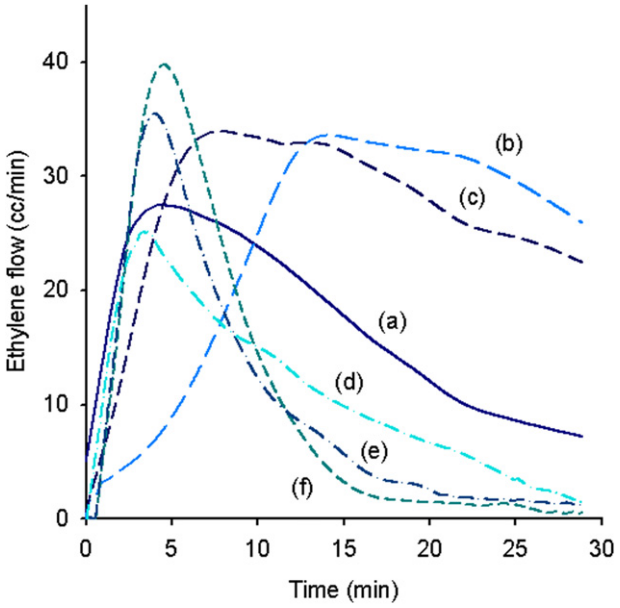

Fig. 4. Plots of rate of ethylene consumption versus time of ethylene oligomerization with sterically modulated catalysts: (a) $Pd_2Cl_4L^1$ at 30 °C, (b) $Pd_2Cl_4L^2$ at 30 °C, (c) $Pd_2Cl_4L^3$ at 30 °C, (d) $Pd_2Cl_4L^1$ at 50 °C, (e) $Pd_2Cl_4L^2$ at 50 °C, and (f) $Pd_2Cl_4L^3$ at 50 °C. Conditions: catalyst = 5 μmol; [EASC]/[Pd] = 300; toluene solvent = 80 mL; $P_{C_2H_4}$ = 1.3 bar; reaction time = 30 min.

Table 1
Results of ethylene oligomerization with $Pd_2Cl_4L^1$, $Pd_2Cl_4L^2$, and $Pd_2Cl_4L^3$ catalysts combined with (EASC). Conditions: catalyst = 5 μmol; [EASC]/[Pd] = 300; toluene solvent = 80 mL; $P_{C_2H_4}$ = 1.3 bar; reaction time = 30 min.

Entry	Catalyst	Temp. (°C)	R_p[a]	Distribution of olefins[b] (in %)					
				C_4	α-C_4	C_6	C_8	C_{10}	C_{12-20}
1	$Pd_2Cl_4L^1$	30	331.2	72.9	96.1	13.6	4.6	5.3	3.6
2	$Pd_2Cl_4L^2$	30	806.8	75.3	78.8	7.3	7.3	8.8	1.3
3	$Pd_2Cl_4L^3$	30	1308.4	79.6	44.3	11.3	5.1	1.9	2.1
4	$PdCl_2L^3$	30	920.1	91.1	33.2	6.4	2.2	0.3	0.0
5	$Pd_2Cl_4L^1$	50	142.6	88.8	13.7	8.3	2.9	0.0	0.0
6	$Pd_2Cl_4L^2$	50	263.6	87.8	14.3	10.1	2.1	0.0	0.0
7	$Pd_2Cl_4L^3$	50	431.6	81.3	12.1	9.3	3.3	1.8	4.3
8	$PdCl_2L^3$	50	118.4	92.7	12.0	6.6	0.7	0.0	0.0

[a] Rate of polymerization in kg-oligomer mol-Pd^{-1} bar^{-1} h^{-1}.
[b] Determined by GC using calibration curves with standard solutions.

maximum hindrance offered by the ligand system will not allow the monomer units to enter from axial positions, by which chain termination occurs after polymer formation. However, in the present group X systems, a similar obstruction is offered by the substituents present on di-anilines, whereas the antipyrine unit has a planar phenyl ring, which cannot prohibit the axial monomer insertion that results in the formation of desired oligomers.

In combination with EASC, all complexes selectively afforded dimerization and trimerization of ethylene along with small amounts of tetramerized product and trace amounts higher olefins. The product distribution is summarized in Table 1. All the three Pd complexes give high butene content as nearly 75% of the total oligomer content. 96, 79, and 44% of total C_4 content formed by $Pd_2Cl_4L^1$, $Pd_2Cl_4L^2$, and $Pd_2Cl_4L^3$, respectively, are found to be 1-butene. $Pd_2Cl_4L^1$ produces the greatest level of 1-butene. Aside from C_4 composition, 5%–10% of the total oligomers produced consist of C_6 and C_8 products. Finally traces of higher olefin content are also detected with all the Pd catalysts.

Yield of the ethylene oligomers and their distributions are also given in Table 1. An increase in the temperature of oligomerization increases to 50 °C produced a sharp (3–4 fold) decrease in activity. The decrease in activity is attributed to the deactivation of active sites and the increase in the entropy of monomer units. At 50 °C, the amount of the C_4 fraction increases to some extent but the selectivity toward 1-butene decreases sharply, demonstrating the activation of various isomerization reactions at high temperature together with oligomerization. The formation of higher olefins is also reduced, as expected.

The oligomerizations were also carried out with mononuclear complex: $PdCl_2L^3$ in similar conditions. Comparing with the results obtained by $Pd_2Cl_4L^3$, it gives lower activity and produces lower level of 1-butene. In addition, the activity decreases about 8 fold by the increase of the temperature from 30 to 50 °C. Although it is too premature to conclude with the data collected here, all of these results may be come from the synergistic effects of the binuclear complexes.

3.3. Detection of active species

As all the Pd catalysts are NMR active, a deeper insight can be gained as regards the nature of active species responsible for the oligomerization. ^1H NMR spectra of the catalysts were recorded under ethylene oligomerization conditions over −2–14 ppm as a function of time. The representative spectra of $Pd_2Cl_4L^1$ are shown in Fig. 5. It is rather difficult to obtain the spectrum of the reaction mixture immediately after the addition of EASC, hence the first scan is observed after 5 min. The spectrum is quite complicated due to the vigorous reaction that occurs between the Pd catalyst and EASC.

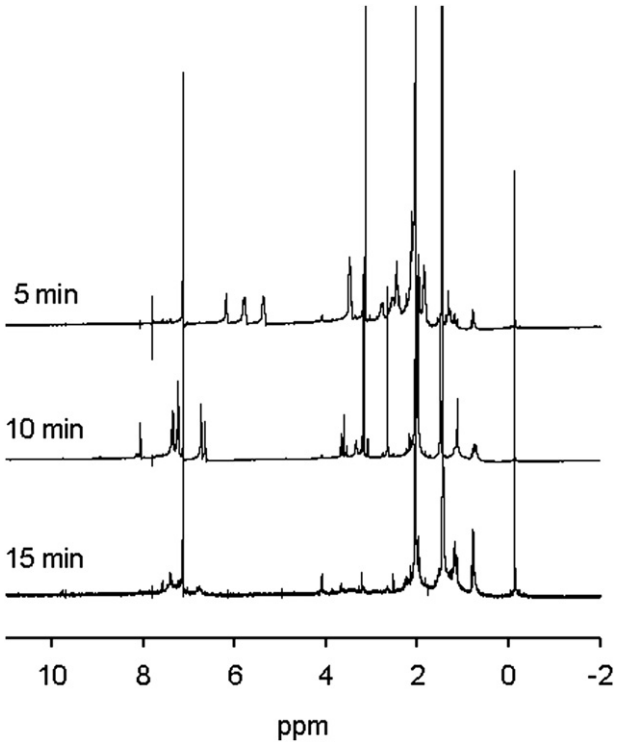

Fig. 5. ^1H NMR spectra of the mixture of $Pd_2Cl_4L^1$, EASC and ethylene, recorded at different reaction periods.

However, important conclusions can be drawn from this spectral observation, since the peaks assigned to Pd complex can be observed, regardless of the complexity of the peaks. After 15 min, the peak intensities are decreased nearly by five times, indicating that the amount of unreacted Pd catalyst decreases as a function time and interestingly, no additional peaks are observed. The decrease of peak intensity in the presence of same amount of mixture indicates the formation of an NMR inactive species due to the change of the geometry of Pd complex. Most probably, this "NMR unresponsive" compound is the active Pd species possessing tetrahedral geometry. Presumably it can be formed by the reaction of the Pd complex and EASC in the presence of ethylene monomer. For example, a diethyl palladium species with tetrahedral geometry having sp^3 hybridization can be formed. The feasibility of the formation of tetrahedral geometry can also be postulated from the cyclic voltammetry results, especially for $Pd_2Cl_4L^1$.

In order to collect more evidence on the formation of active sites, UV–visible spectra of the Pd catalysts were recorded under ethylene oligomerization conditions over the range of 1000 to 200 nm as a function of time. The *d*–*d* transitions originating from square-planar Pd centers are found at around 450 nm (see Experimental). Addition of EASC to the Pd catalyst in toluene, leads to a decrease in *d*–*d* transition and a new absorption at ~800 nm is observed due to the formation of the tetrahedral Pd species. If the square-planar symmetry is maintained, the *d*–*d* transition should be observed in higher energy regions. On the other hand, in case of tetrahedral intermediates, the plane of symmetry can be totally ignored. This observation is consistent with previous studies [28,29].

4. Conclusions

The synthesis and results of spectroscopic and structural characterizations of a new family of sterically modulated binuclear Pd complexes suitable for ethylene oligomerization were presented.

The Pd complexes produced C_4, C_6, C_8, C_{10}, and higher olefin fractions in high activity (up to 1308 kg-oligomer mol-Pd^{-1} bar^{-1} h^{-1}) at 30 °C in combination with EASC. Ligands could be synthesized by the condensation reaction of 4,4′-methylene bis-(2,6-dialkyl aniline) and antipyrine-4-carboxaldehyde in low yields; however, all the Pd complexes were successfully prepared by a one-pot method in good yield. The electrochemical study of the catalysts using CV in DMF solution indicated the presence of single electron transfer redox behavior, leading to a change in the geometry of the Pd complex from square planar to tetrahedral and vice versa. The change from the original NMR active square-planar geometry to the NMR inactive tetrahedral geometry under the oligomerization conditions is the major reason for the high activity of the binuclear complexes.

Acknowledgments

This work was supported by grants-in-aid for the World Class University Program (No. R32–2008–000–10174–0) and the National Core Research Center Program from MEST (No. R15–2006–022–01001–0).

References

[1] C. Bianchini, G. Giambastiani, L. Luconi, A. Meli, Coord. Chem. Rev. 254 (2010) 431–455.
[2] D. Takeuchi, Dalton Trans. 39 (2010) 311–328.
[3] T. Agapie, Coord. Chem. Rev. 255 (2011) 861–880.
[4] (a) Y.D.M. Champouret, J.D. Maréchal, I. Dadhiwala, J. Fawcett, D. Palmer, K. Singh, G.A. Solan, Dalton Trans. (2006) 2350–2361;
(b) Y.D.M. Champouret, J.D. Maréchal, R.K. Chaggar, J. Fawcett, K. Singh, F. Maseras, G.A. Solan, New J. Chem. 31 (2007) 75–85;
(c) G.A. Griffith, M.J. Al-Khatib, K. Patel, K. Singh, G.A. Solan, Dalton Trans. (2009) 185–196;
(d) A.P. Armitage, Y.D.M. Champouret, H. Grigoli, J.D.A. Pelletier, K. Singh, G.A. Solan, Eur. J. Inorg. Chem. (2008) 4597–4607;
(e) Q. Khamker, Y.D.M. Champouret, K. Singh, G.A. Solan, Dalton Trans. (2009) 8935–8944.
[5] (a) K. Kurtev, A. Tomov, J. Mol. Catal. 88 (1994) 141–150;
(b) A. Tomov, K. Kurtev, J. Mol. Catal. A: Chem. 103 (1995) 95–103;
(c) D. Zhang, G.X. Jin, Organometallics 22 (2003) 2851–2854;
(d) X. Mi, Z. Ma, L. Wang, Y. Ke, Y. Hu, Macromol. Chem. Phys. 204 (2003) 868–876;
(e) H.K. Luo, H. Schumann, J. Mol. Catal. A: Chem. 227 (2005) 153–161;
(f) T. Hu, L.M. Tang, X.F. Li, Y.S. Li, N.H. Hu, Organometallics 24 (2005) 2628–2632;
(g) M. Tanabiki, K. Tsuchiya, Y. Motoyama, H. Nagashima, Chem. Commun. (2005) 3409–3411;
(h) J.P. Taquet, O. Siri, P. Braunstein, R. Welter, Inorg. Chem. 45 (2006) 4668–4676;
(i) S. Zhang, W.H. Sun, X. Kuang, I. Vystorop, J. Yi, J. Organomet. Chem. 692 (2007) 5307–5316;
(j) P. Wehrmann, S. Mecking, Organometallics 27 (2008) 1399–1408;
(k) B.A. Rodriguez, M. Delferro, T.J. Marks, J. Am. Chem. Soc. 131 (2009) 5902–5919;
(l) B.K. Bahuleyan, K.J. Lee, S.H. Lee, Y. Liu, W. Zhou, I. Kim, Catal. Today (2010). doi:10.1016/j.cattod.2010.10.084.
[6] R. Chen, J. Bacsa, S.F. Mapolie, Polyhedron 22 (2003) 2855–2861.
[7] J. Skupinska, Chem. Rev. 91 (1991) 613–648.
[8] X.W. Wang, Y.Q. Zheng, Inorg. Chem. Commun. 10 (2007) 709–712.
[9] (a) R.C. Maurya, P. Shukla, J. Inst. Chemists. (India) 69 (1997) 46–48;
(b) R.C. Maurya, D.D. Mishra, M. Pandey, P. Shukla, Natl. Acad. Sci. Lett. (India) 14 (1991) 383–385.
[10] D.S. McGuinness, P. Wasserscheid, W. Keim, C.H. Hu, U. Englert, J.T. Dixon, C. Grove, Chem. Commun. (2003) 334–335.
[11] T. Agapie, S.J. Schofer, J.A. Labinger, J.E. Bercaw, J. Am. Chem. Soc. 126 (2004) 1304–1305.
[12] B.K. Bahuleyan, U. Lee, C.S. Ha, I. Kim, Appl. Catal. A: Gen. 351 (2008) 36–44.
[13] B.M. Trost, A. Fettes, B.T. Shireman, J. Am. Chem. Soc. 126 (2004) 2660–2661.
[14] J. Gao, J.H. Reibenspies, A.E. Martell, Angew. Chem. Int. Ed. 42 (2003) 6008–6012.
[15] S. Budagumpi, V.K. Revankar, Transition Met. Chem. 35 (2010) 649–658.
[16] S.P. Meneghetti, P.J. Lutz, J. Kress, Organometallics 18 (1999) 2734–2737.
[17] L.K. Johnson, C.M. Killian, M. Brookhart, J. Am. Chem. Soc. 117 (1995) 6414–6415.
[18] S. Mecking, L.K. Johnson, L. Wang, M. Brookhart, J. Am. Chem. Soc. 120 (1998) 888–899.
[19] (a) Y.B. Huang, G.R. Tang, G.Y. Jin, G.X. Jin, Organometallics 27 (2008) 259–269;
(b) J.P. Taquet, O. Siri, P. Braunstein, Inorg. Chem. 45 (2006) 4668–4676;
(c) O. Siri, J.P. Taquet, J.P. Collin, M.M. Rohmer, M. Bënard, P. Braunstein, Chem. Eur. J. 11 (2005) 7247–7253.
[20] J. Feldman, S.J. McLain, A. Parthasarathy, W.J. Marshall, J.C. Calabrese, S.D. Arthur, Organometallics 16 (1997) 1514–1516.
[21] D.S. Polycn, I. Shain, Anal. Chem. 38 (1966) 370–375.
[22] J.B. Flanagam, A.J. Bard, F.C. Anson, J. Am. Chem. Soc. 100 (1978) 4248–4253.
[23] B.K. Bahuleyan, G.W. Son, D.W. Park, C.S. Ha, I. Kim, J. Polym. Scienc.: Part A: Polym. Chem. 46 (2008) 1066–1082.
[24] L.E. Breyfigle, C.K. Williams, V.G. Young Jr., M.A. Hillmyer, W. Tolman, Dalton Trans. (2006) 928–936.
[25] H. Li, L. Li, D.J. Schwartz, M.V. Metz, T.J. Marks, L. Liable-Sands, A.L. Rheingold, J. Am. Chem. Soc. 127 (2005) 14756–14768.
[26] D. Chandran, C. Bae, I.Y. Ahn, C.S. Ha, I. Kim, J. Organomet. Chem. 694 (2009) 1254–1258.
[27] S.A. Svejda, M. Brookhart, Organometallics 18 (1999) 65–74.
[28] F. Peruch, H. Cramail, A. Deffieux, Macromolecules 32 (1999) 7977–7983.
[29] D. Chandran, C.H. Kwak, J.M. Oh, I.Y. Ahn, C.S. Ha, I. Kim, Catal. Lett. 125 (2008) 27–34.